Transparent, lightweight and high strength polyethylene films by a scalable continuous extrusion and solid-state drawing process

Yunyin Lin, Wei Tu, Rob C. P. Verpaalen, Han Zhang, Cees W. M. Bastiaansen[*]*, Ton Peijs*[*]

Y. Lin, Dr. H. Zhang, Prof. C. W. M. Bastiaansen

School of Engineering and Materials Science

Queen Mary University of London

Mile End Road, London E1 4NS, U.K.

Dr. W. Tu, Dr. H. Zhang

Nanoforce Technology Ltd.

Mile End Road, London E1 4NS, U.K.

R. C. P. Verpaalen, Prof. C. W. M. Bastiaansen

Laboratory of Functional Organic Materials and Devices

Eindhoven University of Technology

P.O. Box 513, Eindhoven 5600 MB, Netherlands

E-mail: c.w.m.bastiaansen@tue.nl

Prof. T. Peijs

Materials Engineering Centre

WMG, University of Warwick

Coventry CV4 7AL, U.K.

E-mail: t.peijs@warwick.ac.uk

Keywords

polyethylene, film extrusion, orientation, transparency, mechanical properties

Abstract

The continuous production of transparent high strength ultra-drawn high-density polyethylene (HDPE) films or tapes is explored using a cast film extrusion and solid-state drawing line. Two methodologies have been explored to achieve such high strength transparent polyethylene films; (i) the use of suitable additives like 2-(2H-benzotriazol-2-yl)-4,6-ditertpentylphenol (BZT) and (ii) solid-state drawing at an optimal temperature of 105 °C (without additives). Both methodologies result in highly oriented films of high transparency (~ 91 %) in the far field. Maximum attainable modulus (~ 33 GPa) and tensile strength (~ 900 MPa) of both types of solid-state drawn films are similar and are an order of magnitude higher than traditional transparent plastics such as polycarbonate (PC) and poly(methyl methacrylate) (PMMA). Special emphasis is devoted to the effect of draw down and pre-orientation in the as-extruded films prior to solid-state drawing. It is shown that pre-orientation is beneficial in improving mechanical properties of the films at equal draw ratios. However, pre-orientation lowers the maximum attainable draw ratio and as such the ultimate modulus and tensile strength of the films. Potential applications of these high strength transparent flexible films lie in composite laminates, automotive or aircraft glazing, high impact windows, safety glass and displays.

Graphic for the Abstract

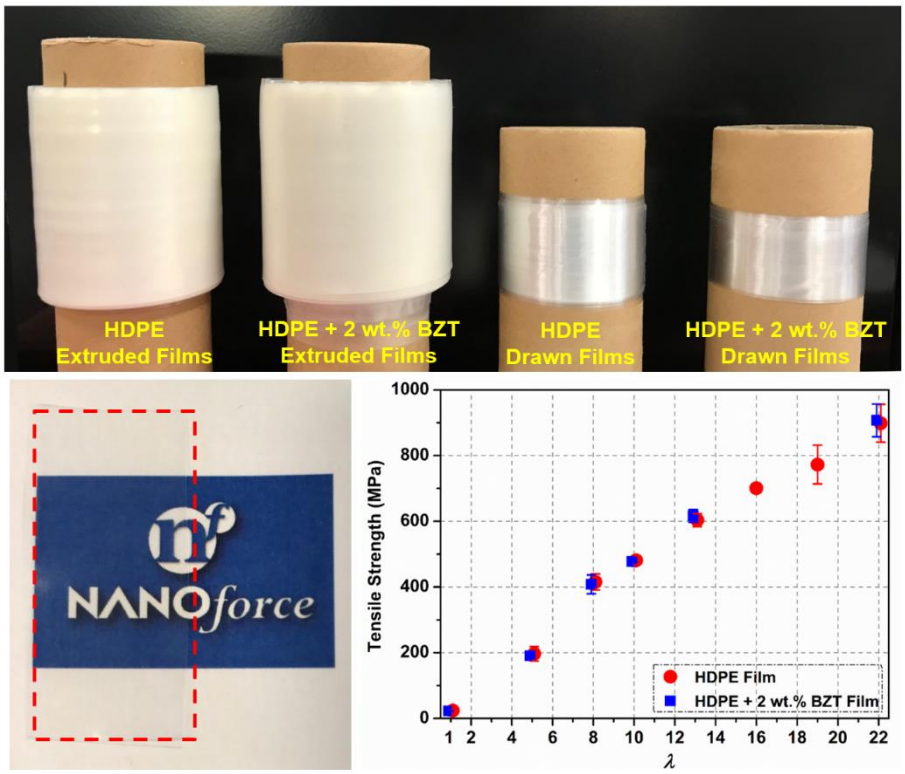

1. Introduction

Common transparent amorphous polymeric materials such as polycarbonate (PC) and poly(methyl methacrylate) (PMMA) are extensively used in high impact windows and transparent armor applications as single layer materials or as multi-layer laminates.[1-7] However, due to their relatively low modulus (< 3 GPa) and strength (< 0.1 GPa),[8] impact properties of these polymeric materials are usually moderate in comparison to laminated glass with polymeric interlayers such as vinyl layers as ethylene-vinyl acetate (EVA), polyvinyl butyral (PVB) or thermoplastic polyurethane (TPU)[9-13] or non-transparent high-performance composite laminates based on aramid or ultra-high molecular weight polyethylene (UHMWPE) fibers.[14-20]

A low-cost but effective post-processing method to increase the stiffness and tensile strength of polymeric materials, notably semi-crystalline polymers, is by stretching or drawing. Even in the case of aircraft windows moderately stretched (amorphous) acrylic is used since it provides better resistance to crazing and improved impact resistance to cast sheet. Existing transparent high-density polyethylene (HDPE) films and sheets are mostly drawn or blown in the melt state. Since chain relaxation and entropy prevents effective chain orientation and chain extension in the melt, these melt-stretched or melt-blown HDPE films possess moderate levels of molecular orientation and similarly low moduli (~ 4 GPa) and strengths (~ 0.2 GPa) as isotropic PC and PMMA.[21-23]

In order to create the next generation high impact transparent windows for transport, life protection and building applications,[6, 19, 24] there is a clear need to create a step-change in performance of transparent polymeric films and sheets with mechanical properties significantly improved compared to plastics like PC or PMMA.

Recently, Shen *et al.* added a 2-(2H-benzotriazol-2-yl)-4,6-ditertpentylphenol (BZT) additive to HDPE films which were drawn to high draw ratios (~ 20), resulting in highly oriented polymer films with transmittance values of 90 % and a tensile strength of 650 MPa.[25, 26] BZT additives are typically used in small amounts (< 1 %) as UV absorbers for polymers and coatings. Shen *et al.* on the other hand added slightly larger amounts (up to 5 %) of BZT to induce transparency in drawn HDPE films. As these additives have similar refractive indices as HDPE, they can eliminate light scattering by filling voids or defect structures induced in the films by the solid-state drawing process, hence lowering the refractive index mismatch between polymer and voids, and thus leading to improved transparency of these oriented films.

More recently, it was discovered that highly transparent ultra-drawn HDPE films with similar high mechanical properties could also be obtained by drawing these films in a specific

temperature window in the solid-state to a draw-ratio of around 20.[27, 28] A transmittance of 90 % in the visible light range was achieved in both the near and far field and a high modulus and strength of 27 GPa and 800 MPa were obtained when drawing was performed in a temperature window between 90 °C and 110 °C. It was demonstrated that solid-state drawing within this temperature window close to but below the melting temperature reduced the formation of fibrillar surface relief structures and avoided the formation of microvoids in the bulk of the film, which eliminates the need for additives like BZT.

In the above-described studies either with[25, 26] or without additives[27, 28] lab-scale and batch-wise fabrication procedures were employed to produce the oriented transparent HDPE films. These procedures involved micro-compounding in the case of additives, compression molding of films followed by solid-state drawing using a universal tensile tester equipped with a thermostatically controlled environmental chamber. Although a proof-of-principle was established, the process only yielded narrow (< 0.5 cm) films or tapes of limited length (< 30 cm), which seriously limits the use and evaluation of these films in single or multi-layer laminates of larger dimensions.

In this study, a cast film extrusion and solid-state stretching line was employed for the scalable and continuous production of oriented HDPE films of high transparency and strength. The benefit of this processing approach lies in the use of conventional polymer processing equipment, which allows for a direct implementation into an industrial environment. The effects of using a specific drawing temperature as well as the addition of BZT on the degree of molecular orientation and microstructure, and optical and mechanical performance of the drawn HDPE films are explored. In addition, the influence of pre-orientation as a result of extrusion draw down and two-step drawing is investigated as these variables could not be investigated in the batch-wise process as described earlier.

2. Experimental Section

2.1. Materials

The high-density polyethylene (HDPE) grade used in this study was Borealis VS4580 (Borealis AG, Austria) with a melting temperature (T_m) of 134 °C, a pellet density of 0.958 g cm^{-3} and a melt flow index (MFI) of 0.6 g/10 min at 190 °C/2.16 kg and 21 g/10 min at 190 °C/21.6 kg. The selected HDPE grade was based on earlier work on the effect of polymer grade on drawability and ultimate mechanical properties of polyethylene fibers.[29-31] 2-(2H-benzotriazol-2-yl)-4,6-ditertpentylphenol (BZT) with molecular formula of $C_{22}H_{29}N_3O$ and a density of 1.170 g cm^{-3} was provided by BASF (Germany, TINUVIN® 328). According to the datasheet of TINUVIN® 328, the weight loss of pure BZT substance is 1.0 % at a temperature of 183 °C measured with thermal gravimetric analysis (TGA) at a heating rate of 20 °C/min in air. Thermoplastic polyurethane (TPU) ST-6050 sheets were supplied by Schweitzer-Mauduit International, Inc. (USA).

2.2. Processing

For producing HDPE pellets with 2 wt.% BZT, a Dr. Collin ZK 25 × 40 (Germany) laboratory twin-screw compounder was used at 80 rpm and a die temperature of around 175 °C. At this mixing temperature, the weight loss of BZT particles is less than 1.0 % of the total amount of BZT which means that BZT has a high stability at this temperature. The BZT concentration used was based on a previous study by Shen *et al.*[25] who showed that drawn HDPE films containing 2 wt.% BZT could already transmit 90 % of visible light. After compounding, the extruded melt was cooled in a water bath and cut into pellets using a Dr. Collin CSG171 (Germany) strand pelletizer. The throughput of the compound was 1.5 kg hr^{-1}.

A Dr. Collin E20T (Germany) single screw extruder was used to extrude HDPE films as shown in ***Figure 1(a)***. A melt pump was used to control the throughput. The single screw extruder was operated at 45 rpm while the temperature of the slot die was around 200 °C. The extruded films were cooled by an X'plore (Netherlands) air knife before being collected using a flat-film take-off unit (Dr. Collin CR72T, Germany). The width and thickness of the slot die was 10 cm and 0.30−0.45 mm, respectively. The winding speed of the collector was about 0.6 m min^{-1}. The average thickness (*t*) of the extruded films was calculated by the following equation:

$$t\ (\mu m) = \frac{\rho_l (dtex)}{\rho (g\ cm^{-3}) \times w\ (cm) \times 100} \quad (1)$$

where ρ_l is the linear density of the extruded films, which is measured by weighing a certain length of film, ρ is the density of the films (0.958 g cm^{-3} for neat HDPE and 0.962 g cm^{-3} for HDPE + 2 wt.% BZT) and *w* is the width of the films.

An initial drawing process often called draw down which predominantly occurs in the melt will take place during cast film extrusion.[32, 33] The draw down or pre-orientation ratio (λ_{pre}), was calculated using the following equation:

$$\lambda_{pre} = \frac{w_{slot} \times t_{slot}}{w_{extruded} \times t_{extruded}} \quad (2)$$

where w_{slot}, t_{slot}, $w_{extruded}$ and $t_{extruded}$ denote the width or thickness of the slot die or extruded films, respectively. The obtained thickness of as-extruded cast films after draw down (λ_{pre} = 4) was generally in the range of 100−200 μm.

The as-extruded HDPE films with and without BZT additives were subsequently drawn in the solid-state using a Dr. Collin MDO-A & MDO-B (Germany) uniaxial stretching line as shown in ***Figure 1(b)***. Based on our previous research,[27] the solid-state drawing temperature was chosen at 105 °C in order to achieve highly transparent high strength HDPE films without the

need to incorporate additives. The rotating speed of the rollers in part I and part II depended on the requested draw ratio, usually 0.10−0.20 m min^{-1} and 1.0−2.2 m min^{-1}, respectively. The machine direction (MD) corresponds to the drawing direction.

The average thickness (t) of the drawn films was also calculated by Equation (1), usually about 20−40 μm on the basis of the solid-state draw ratio (λ), which was calculated by the following equation:

$$\lambda = \frac{w_{extruded} \times t_{extruded}}{w_{drawn} \times t_{drawn}} \quad (3)$$

where $w_{extruded}$, $t_{extruded}$, w_{drawn} and t_{drawn} are the width or thickness of extruded films or drawn films, respectively.

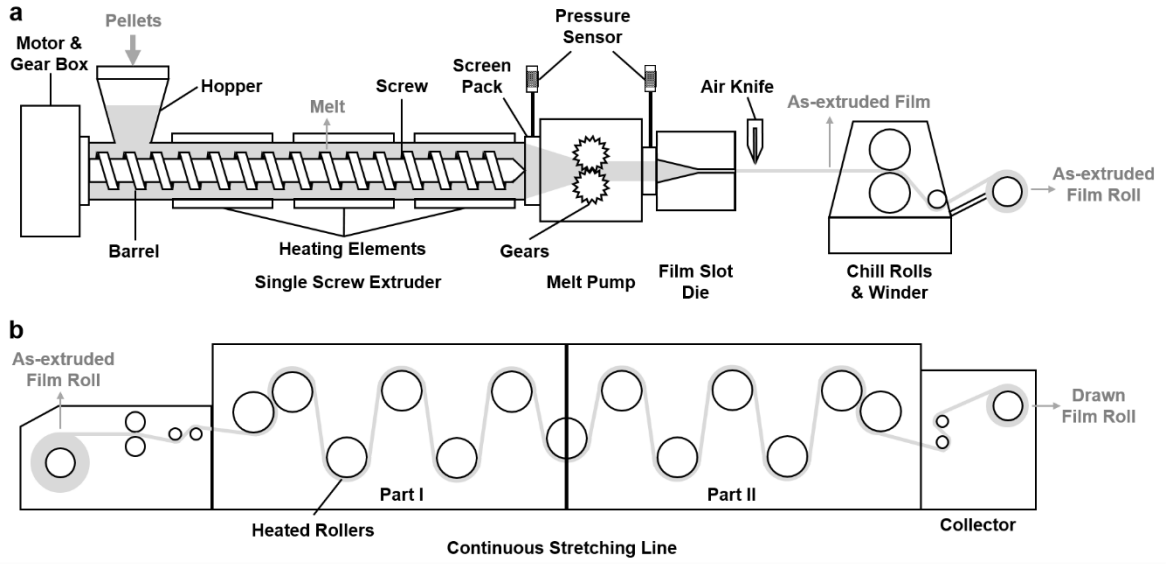

Figure 1. Schematic diagram of (a) cast film extrusion and (b) solid-state drawing.

In case of two-step drawing, the extruded films were drawn twice in the solid-state. For instance, films were first drawn to a draw ratio of 5 followed by a draw ratio of 2, making a total λ = 10. The draw ratios of the 1st and 2nd drawing are called λ_1 and λ_2, respectively, i.e. λ_1 = 5 and λ_2 =

2 as in the above case. The drawing temperature in this multi-stage drawing process was again kept constant at 105 °C.

For purposes of comparison, isotropic compression molded HDPE films (λ_{pre} = 1 and λ = 1) with a thickness of ~ 100 μm were prepared using a Dr. Collin P300E (Germany) hot press at 160 °C for 3 min and then cooled down to room temperature (RT).

In order to eliminate light scattering from surface roughness effects,[25, 27] HDPE films with and without additives were sandwiched between two glass slides using TPU films as interlayers when testing optical performance. Compression molding of these laminated structures was carried out in a Rondol (UK) hot press at 100 °C, 3 bar for 5−10 min.

2.3. Characterization

Transmittance spectra of laminates based on drawn HDPE films with and without additives were acquired using a PerkinElmer Lambda 950 (USA) UV-vis spectrometer in the wavelength regime of 400−700 nm at an interval of 1 nm. A sample-to-detector distance of 40 cm was used in order to obtain transmittance values in the far field rather than near field. In literature, optical transparency is often claimed by placing a "transparent" sample directly on top of a background image (near field). However, real transmittance usually refers to the ability of an observer to "see-through" a relatively distant sample, analogous to seeing through a window (far field). Here, the optical transmittance of the laminated samples is measured when placed at a distance from the detector (40 cm), which as mentioned earlier is of greater practical importance for potential applications like glazing or windows.[27] Transmittance measurements were carried out at least three times for each film.

Small-angle light scattering (SALS) of the laminated samples was carried out using a JDS Uniphase (USA) 15 mW Helium-Neon gas laser at a steady intensity with a wavelength of 633 nm as a light source. The sample-to-screen distance was fixed at 15.5 cm. The tested range of scattering vector (q) was 0.6−6 μm^{-1}, and therefore the corresponding detectable microvoid size is around 3−25 μm.[34] V_v polarization patterns were obtained with the polarizer and the analyzer set parallel to each other. The laminated samples were placed between polarizers with the MD of the oriented films perpendicular to the polarizers. The scattering vector (q) is calculated by the following equation:

$$q = \frac{4\pi \times \sin\theta}{\lambda} \tag{4}$$

where 2θ is the scattering angle and λ is the wavelength.

Young's modulus and tensile strength of the films were measured using an Instron 5566 (UK) universal tensile tester with manual wedge action grips at RT according to ASTM D882-18 standard. Rectangular test specimens with gauge dimensions of 100 mm × 10 mm were carefully cut from the films. The tensile tests were carried out at a pre-load of 0.2 N and at a crosshead speed of 50 mm min^{-1}. Young's modulus was calculated from the tangent of the engineering stress-strain curve at a strain < 0.5 %. The average Young's modulus and tensile strength as well as their standard deviation were calculated using a minimum of three specimens.

Scanning electron microscopy (SEM) of HDPE films was carried out using a FEI Inspect F (Netherlands) at an acceleration voltage of 5 kV. Energy-dispersive X-ray spectroscopy (EDS) was measured using spot scan mode in combination with SEM. Wide-angle X-ray scattering (WAXS) and small-angle X-ray scattering (SAXS) were all carried out using a SAXSLAB Ganesha 300XL instrument (Denmark) with a Genix-Cu ultralow divergence source, which

could emit X-ray photons with a wavelength of 1.54 Å at a flux of 10^8 photons per second. Diffraction patterns of the films were collected on a Dectris Pilatus 300K silicon pixel detector with 487 × 619 pixels. The detector possessed three plates with a total area of 172 μm^2 and intervals between each of the plate was 17 pixels, leading to two straight dark bands in the diffraction pattern. The sample-to-detector distance was 91 mm for WAXS and 1491 mm for SAXS, respectively. The q range of SAXS test was 0.006−0.1 Å^{-1}, which corresponds to a detectable nanovoids' dimension (d) of less than 105 nm as estimated by equation $d = 2\pi/q$.[35, 36] The beam center and the scattering vector (q) of the WAXS and SAXS images were calibrated using the diffraction peaks of a silver behenate (AgBeh) standard in SAXSGUI software, while the q value was calculated by Equation (4).

Crystallinity (X_c) could be calculated from the WAXS data using the following equation:[25]

$$X_c = \frac{I_{110}+1.46I_{200}}{I_{110}+0.75I_a+1.46I_{200}} \times 100\% \quad (5)$$

where I_{110}, I_a and I_{200} denote the integrated areas of the (110), amorphous and (200) peak of polyethylene, respectively.

Hermans' orientation factor (f_c) is usually used to quantify the degree of the orientation of drawn polymeric samples.[37, 38] For uniaxial orientation along the MD, f_c was calculated from the WAXS data using the following equation:

$$f_c = \frac{3<\cos^2\beta_c>-1}{2} \quad (6)$$

where β_c is the angle between the chain axis and the MD. For polyethylene, $<cos^2\beta_c>$ equals to[38]:

$$<\cos^2\beta_c> = 1 - 0.565 <\cos^2\beta_{200}> - 1.435 <\cos^2\beta_{110}> \quad (7)$$

where β_{110} and β_{200} are the angles between the MD and (110) or (200) peak, and $<cos^2\beta_x>$ is defined by the following equation:

$$< \cos^2 \beta_x >= \frac{\int_0^{\frac{\pi}{2}} I(\beta_x) \cos^2 \beta_x \sin \beta_x d\beta_x}{\int_0^{\frac{\pi}{2}} I(\beta_x) \sin \beta_x d\beta_x} \quad (8)$$

where x represents (110) or (200) peak, and $I(\beta_x)$ is the scattering intensity along the angle β_{110} or β_{200}.

The long period (L_p) in HDPE films was calculated by the Bragg equation[39]:

$$L_p = \frac{2\pi}{q_{max}} \quad (9)$$

where q_{max} is the peak value of the scattering vector (q) in the Lorentz-corrected intensity (I) versus scattering vector curve.

Lamellar thickness (L_c) could be estimated from the long period according to a two-phase model using the following equation[40]:

$$L_c = L_p \times X_c \quad (10)$$

where X_c is the crystallinity of the HDPE films measured by WAXS.

3. Results and Discussion

The appearance of the as-extruded HDPE films with and without BZT additive at a draw down or pre-orientation ratio (λ_{pre}) of 4 is milky and opaque as shown in ***Figure 2(a)***, whereas after solid-state drawing at 105 °C to a draw ratio (λ) of 10, the films have quite a clear appearance (***Figure 2(b)***). In ***Figure 2(c)***, the transmittance of the HDPE films significantly increases after solid-state drawing in the visible light wavelength regime. Moreover, both solid-state drawn

HDPE films with and without BZT additive show similar transmittance values at a wavelength of 550 nm at equal draw ratios (***Figure 2(d)***). A wavelength of 550 nm within the visible spectrum was chosen as this is the most sensitive wavelength to the human eye. It is noteworthy that a transmittance value of nearly 91 % can be achieved for both types of films at high draw ratios ($\lambda \geq 10$) even in the far field, which is close to glass (~ 92 %). This means that solid-state drawing of HDPE films carried out at a temperature of 105 °C and of films with BZT additive in both cases leads to highly transparent HDPE films after drawing. As our previous research already showed,[27] a relatively high drawing temperature facilitates greater chain mobility and the formation of less interfibrillar defects, leading to a reduction in the formation of microvoids in the bulk or on the surface of the films. Suitable additives like BZT, having a similar refractive index to HDPE, can fill such voids and reduce the mismatch of refractive indices between HDPE and the voids.[25] What's more, it was observed that the films reached an optimum transmittance value at λ = 13−16. This phenomenon can be explained by the formation of microvoids and microcracks parallel or perpendicular to the machine direction (MD) at higher draw ratios (λ > 16).[27]

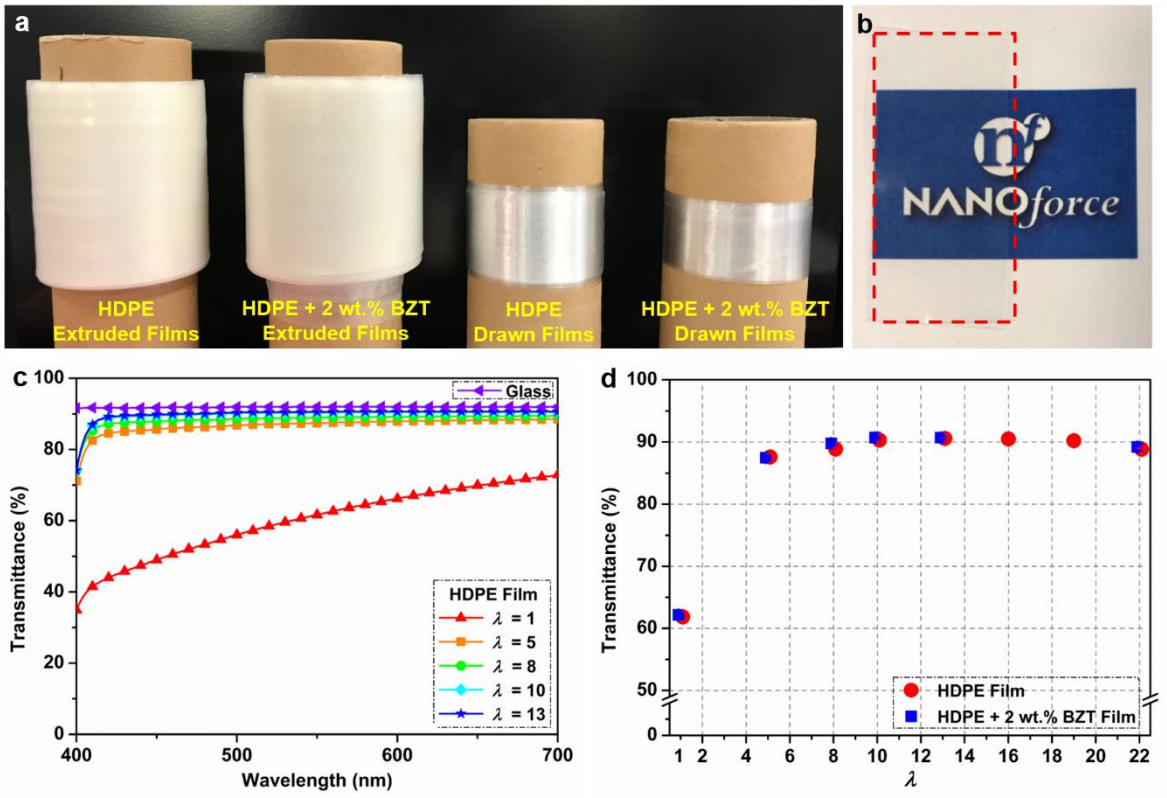

Figure 2. (a) Photographs of as-extruded (λ_{pre} = 4) and drawn (λ = 10) HDPE film rolls with and without BZT additives and (b) the appearance of drawn HDPE films with λ_{pre} = 4 and λ = 10 (marked and located between the dashed red lines), showing a high transparency after solid-state drawing. (c) Transmittance of HDPE films in the visible spectrum range and (d) transmittance of HDPE and HDPE + 2 wt.% BZT films (λ_{pre} = 4) drawn at 105 °C to different draw ratios at a wavelength of 550 nm and a 40 cm sample-to-detector distance (far field), illustrating similar optical performance of films with and without additives when drawn at 105 °C. For transmittance test, the films were sandwiched between TPU interlayers and glass to eliminate surface light scattering effects.

Figure 3 shows the Young's modulus and the tensile strength of solid-state drawn HDPE films with and without BZT additives along the MD as a function of draw ratio. Both modulus and strength increase with draw ratio for both types of HDPE films. The stress-strain curves of ultra-drawn HDPE films with λ = 22 both with and without BZT additive (see Supporting

Information ***Figure S1***) illustrate that the films fail at an elongation of 8−9 % and possess a maximum attainable modulus of ~ 33 GPa and a maximum tensile strength of ~ 900 MPa along the MD. These moduli and strength values are similar to those of unidirectional glass-fibre reinforced plastics but at about half the density. The maximum achievable modulus and strength exceeds nearly 15 times that of common transparent polymeric materials like PC and PMMA. Moreover, on a weight basis these polymeric films even outperform a lightweight engineering materials like aluminum with a specific modulus and tensile strength of, respectively 34 GPa g^{-1} cm^3 and 940 MPa g^{-1} cm^3 for HDPE (along the MD) versus 26 GPa g^{-1} cm^3 and 125 MPa g^{-1} cm^3 for aluminum. Mechanical properties of uniaxially stretched polyethylene films along the transverse direction (TD) are however usually much lower, with typical moduli and strengths of ~ 2 GPa and ~ 15 MPa according to our previous study.[41]

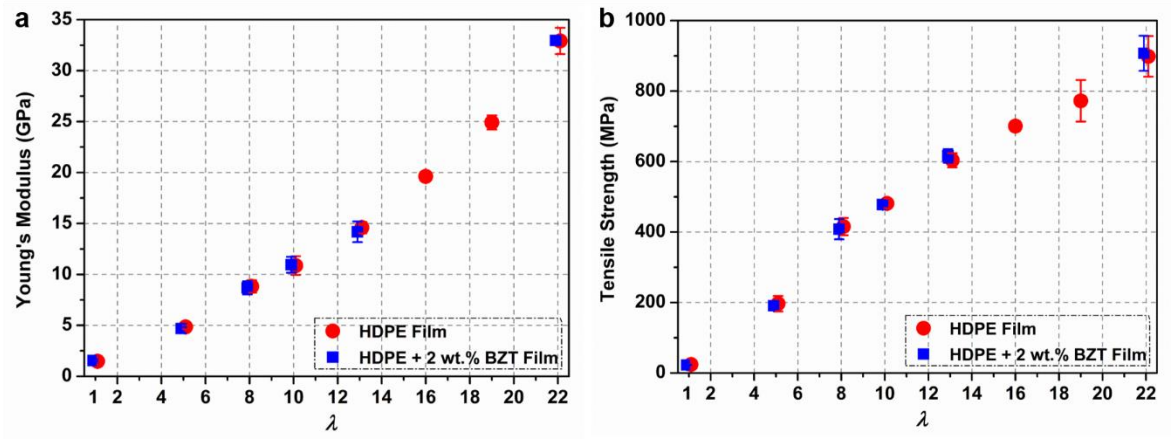

Figure 3. (a) Young's modulus and (b) tensile strength of HDPE films with and without BZT additives (λ_{pre} = 4) along the MD as a function of draw ratio, indicating similar mechanical properties for HDPE films with and without additives when drawn at 105 °C.

SALS under V_v polarization mode is generally carried out to detect light scattering from a perspective of density fluctuations.[42] In ***Figure 4***, relatively weak light scattering can be seen in the drawn HDPE films, indicating that only a small amount of microvoids exist in these

films along the MD. The crystalline phase of HDPE can undergo plastic flow.[43] Quenching results in a weaker crystalline phase which can undergo plastic flow and crystalline block slip.[44, 45] Moreover, drawing at temperatures well above the α-relaxation temperature of polyethylene, which is expected to be around 80 °C, results in greater chain transport and mobility in the crystalline phase and less cavitation.[46, 47] Chain transport avoids the build-up of triaxial stresses between crystals. These stresses are responsible for cavitation and void formation during drawing, leading to light scattering and an opaque appearance of the films. Drawing at temperatures well above the α-relaxation temperature lowers these stresses, leading to highly transparent HDPE films even without the use of additives (see ***Figure 2(b)***). HDPE films with BZT additives show even less scattering after drawing with patterns similar to glass. However, the small amount of light scattering still present in the films without BZT hardly affects the transparency of these films (see ***Figure 2(d)***). Clearly it is the small number of remaining (unfilled) microvoids in both types of HDPE films that is responsible for the high clarity of both films after drawing.

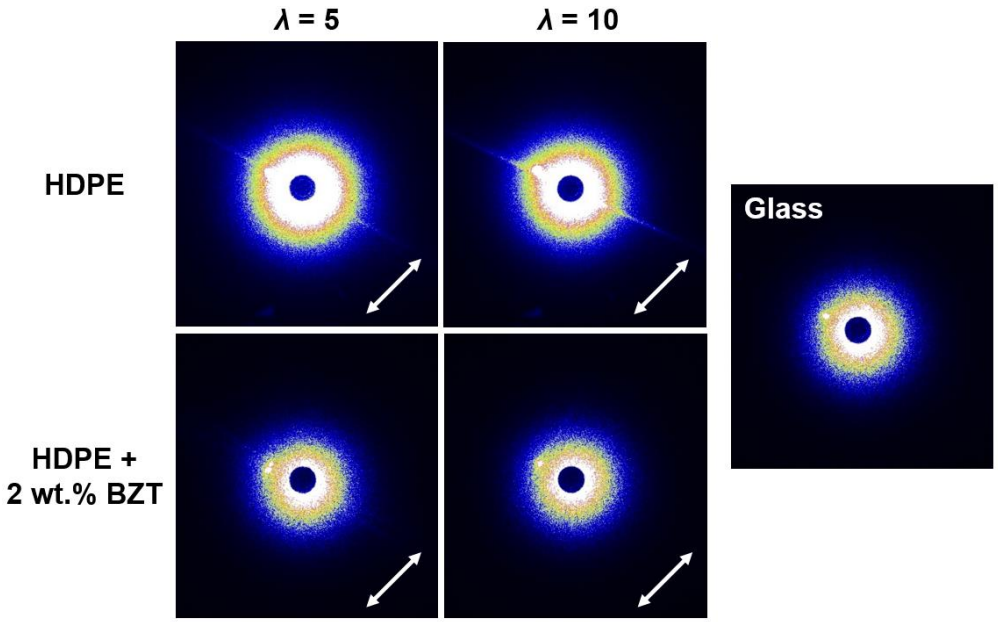

Figure 4. SALS images of glass, drawn HDPE films with and without BZT additives (λ_{pre} = 4) at λ = 5 and λ = 10, indicating negligible light scattering from remaining microvoids for both types of films. The films were sandwiched between glass and TPU interlayer to eliminate surface light scattering effects, and the arrows show the MD of the films.

Although nano-sized defect structures that are smaller than the wavelength of visible light in principle may not contribute to light scattering, these nanovoids might aggregate and develop into microvoids.[48] In the insets of ***Figure 5***, the 2D-SAXS images of extruded HDPE films with and without additives (λ_{pre} = 4, λ = 1) show tear-drop shaped meridional lobes parallel to the MD. This SAXS pattern can be interpreted in terms of a two-phase system of lamellae and amorphous regions, where the stacks of lamellae are slightly oriented perpendicular to the MD in the extrusion process.[38] After solid-state drawing to λ = 10, the 2D-SAXS pattern increases in intensity to a two-point layer-like pattern with two sharp meridional spots situated on each side of the beam stop, illustrating that a highly-aligned lamellar structure is generated.[22] Moreover, a streak-like scattering across the beam stop (indicated by the yellow solid single-headed arrow in the insets of ***Figure 5***) perpendicular to the MD is observed for the drawn films as a result of differences in electron density between polymer and voids together with the formation of a fibrillar structure along the MD after solid-state drawing.[49, 50] The morphology of the extruded HDPE films (λ = 1) with and without BZT additives (shown in ***Figure 6***) does not show a surface structure after pre-orientation, whereas the drawn HDPE films (λ = 10) show a highly fibrillar surface structure after solid-state drawing. Since the fibrillar structure of the drawn HDPE films is similar for the same solid-state draw ratio, the differences in the streak intensity at identical draw ratios is expected to result from the presence of voids parallel to the MD.[31] The scattering vector (q) range of the SAXS test was 0.006−0.1 $Å^{-1}$, corresponding to a detectable nanovoids' dimension (d) of less than 105 nm as estimated by equation $d = 2\pi/q$.[35,

[36] In the corresponding 1D-SAXS curves (***Figure 5***), the one-dimensional scattering intensity (*I*) at low *q* value corresponds to the intensity of the streak. It demonstrates that the scattering intensity of the streak is similar for HDPE films with and without BZT additives at equal draw ratios. This outcome suggests that the lateral and longitudinal dimensions of voids inside both types of films are similar, explaining the high transparency of both solid-state drawn films after drawing at a temperature of 105 °C.

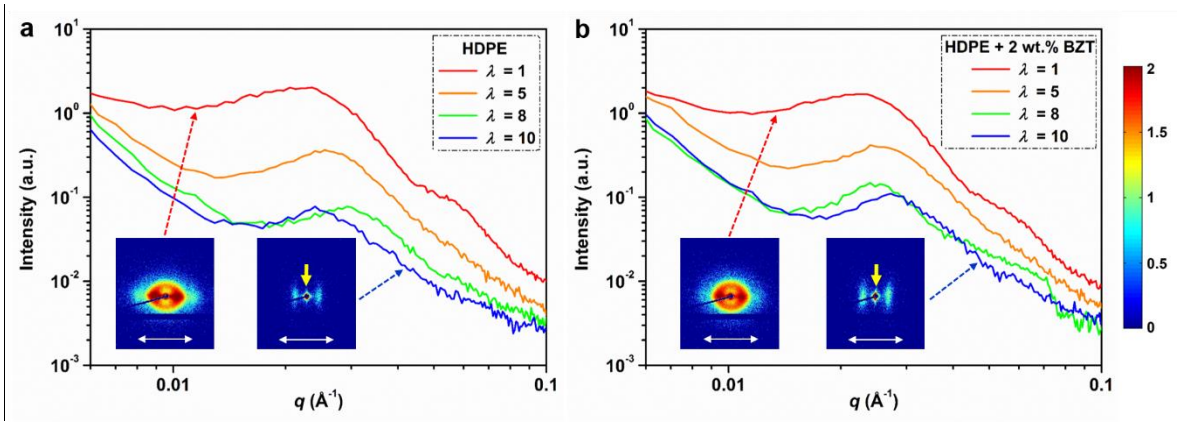

Figure 5. 1D-SAXS curves of scattering intensity in HDPE films (a) with and (b) without BZT additives (λ_{pre} = 4) at different draw ratios as a function of scattering vector, suggesting the presence of only a small amount of nanovoids in both films. The insets are the corresponding 2D-SAXS patterns of films at λ = 1 and λ = 10, the yellow solid single arrows indicate the streak-like scattering while the white double arrows represent the MD.

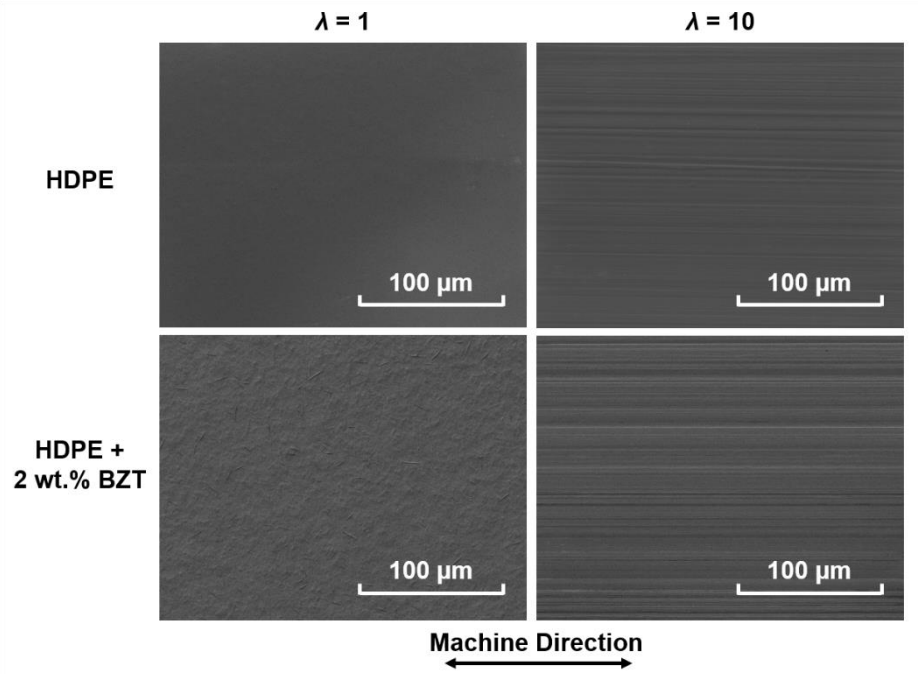

Figure 6. SEM images of the extruded (λ = 1) and drawn (λ = 10) HDPE films with and without BZT additives (λ_{pre} = 4), showing the formation of a fibrillar structure after solid-state drawing.

With increasing draw ratio, typical (110) and (200) reflections of the orthorhombic polyethylene unit cell in the WAXS patterns become more apparent and more oriented as shown in ***Figure 7***. At λ = 1 the WAXS pattern shows a fairly diffuse ring typical for an isotropic semi-crystalline polymer, suggesting negligible molecular orientation, while the film drawn to λ = 10 shows sharp spotty reflections, revealing high chain orientation along the MD for this sample. The Hermans' orientation factor (f_c) in ***Table 1*** increases rapidly at relatively low draw ratios ($\leq$ 5), suggesting higher crystal alignment and chain orientation along the MD with solid-state drawing.[38, 51] Hermans' orientation factor saturates at higher draw ratios, meaning that crystal orientation remains more or less constant at draw ratios above 8.

With solid-state drawing, the long period (L_p) in SAXS disappears. Crystallinity (X_c) partially declines at low draw ratios ($\lambda \leq 5$) which is related to the breakup of lamellar crystallites at the early stages of drawing.[52] Then X_c increases with further drawing because of the

transformation from microfibrils to chain-extended and highly-aligned structures during deformation, leading to a reduction in amorphous regions and therefore an increase in overall crystallinity.[53] Furthermore, it should be noted that WAXS patterns, X_c, f_c, L_p and L_c of HDPE films with and without BZT additives are similar for each draw ratio (***Figure 7*** and ***Table 1***). This means there is little difference in microstructure of both types of HDPE films.

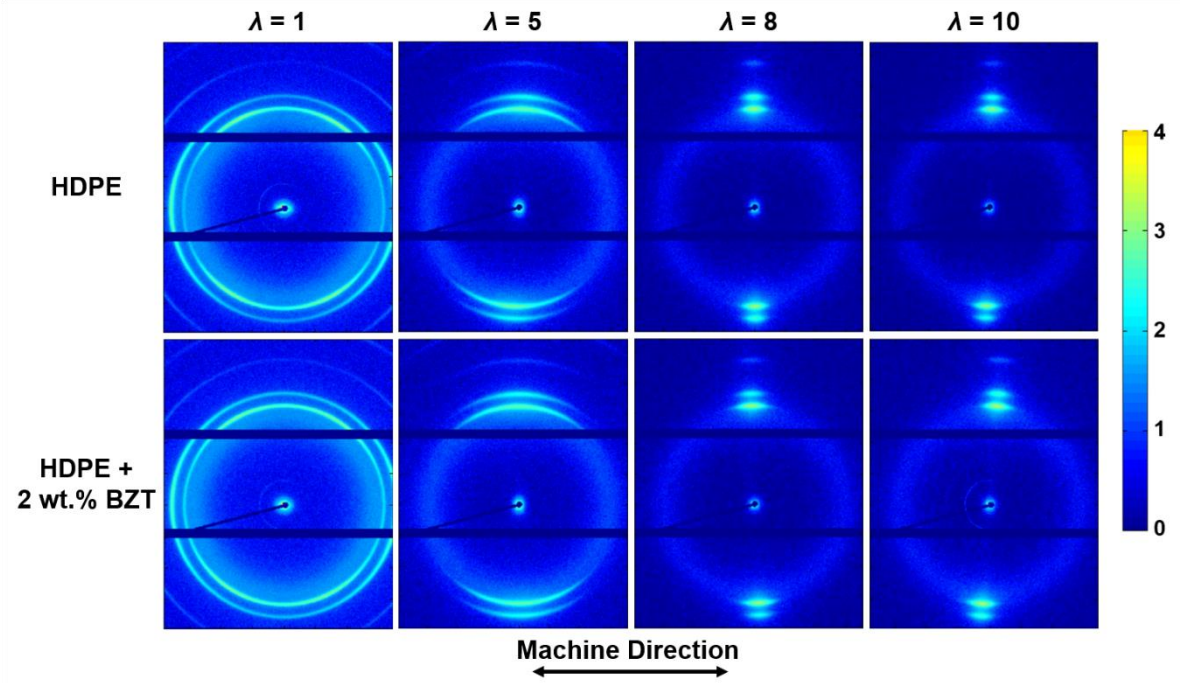

Figure 7. WAXS images of HDPE films with and without BZT additives (λ_{pre} = 4) drawn at 105 °C to different draw ratios, showing a similar transition from isotropic to oriented structure with draw ratio for both types of films.

Table 1. Crystallinity (X_c), Hermans' orientation factor (f_c), long period (L_p) and lamellar thickness (L_c) of HDPE films drawn at 105 °C with and without BZT additives with different pre-orientation ratios (λ_{pre}) and draw ratios (λ) from the WAXS and SAXS data.

HDPE Films	λ_{pre}	λ_1	λ_2	X_c **[%]**	f_c	L_p **[nm]**	L_c **[nm]**
Neat HDPE	4			65.8	/	30.3	19.9
	4	5		62.7	0.805	25.1	15.8
	4	8		63.8	0.896	22.9	14.6
	4	10		65.6	0.911	26.7	17.5
	4	5	2	65.9	0.907	27.5	18.1
	4	19		67.7	0.926	26.7	18.1
	18			68.4	/	29.0	19.8
	18	5		63.0	0.874	26.2	16.5
HDPE + 2 wt.% BZT	4			64.1	/	30.0	19.2
	4	5		62.5	0.803	25.2	15.8
	4	8		64.4	0.894	25.6	16.5
	4	10		65.9	0.907	23.6	15.6

As for the importance of two-step drawing, the transmittance, Young's modulus and tensile strength of films fabricated by such a two-step drawing process were all very similar to those made using a one-step drawing process (***Table 2***). Previous work on polyoxymethylene (POM) which has similar drawing behavior as linear polyethylene (PE) and polypropylene (PP) also suggested that there is no significant advantage of using a two-step drawing process instead of a one-step drawing process in terms of achieving ultimate mechanical properties.[54] The SEM images, WAXS patterns, X_c, f_c, L_p and L_c from ***Table 1*** and ***Figure S2*** show great similarities between them. These results suggest that a two-step drawing process did not significantly alter film morphology, crystallinity, degree of orientation or optical and mechanical properties.

Table 2. Transmittance at 550 nm and mechanical properties of drawn HDPE films (λ_{pre} = 4 and λ = 10) by one-step and two-step drawing process.

HDPE Films	Transmittance [%]	Modulus [GPa]	Strength [MPa]
One-step Drawing	90.3 ± 0.2	10.87 ± 0.92	481 ± 14
Two-step Drawing	90.0 ± 0.2	10.76 ± 0.75	483 ± 34

Figure 8 on the other hand shows that the draw down or pre-orientation ratio (λ_{pre}) has a significant effect on mechanical properties of the films after solid-state drawing. When λ_{pre} is increased, the slope of the modulus and strength versus draw ratio curves becomes significantly steeper (see ***Figure 8(a)*** and ***8(b)***). A more than 55 % increase in Young's modulus and tensile strength of HDPE films at λ = 5 can be observed when λ_{pre} is increased from 4 to 18. WAXS patterns shown in ***Figure 9*** and f_c listed in ***Table 1*** show a much higher degree of chain orientation in the drawn HDPE films with λ_{pre} = 18. Moreover, due to some induced chain pre-orientation during draw down of the melt in cast film extrusion, the strength of these extruded and drawn films is higher than batch-wise processed films as reported in our previous studies.[25, 27] More importantly, the transmittance values of the solid-state drawn HDPE films with different λ_{pre} still remain high (~ 90 %) and barely change with draw ratio as shown in ***Table 3***.

However, the maximum attainable solid-state draw ratio (λ_{max}) of HDPE films is only 10 for λ_{pre} = 12 and 7 for λ_{pre} = 18, respectively. The maximum modulus and strength of the films therefore drops with increasing λ_{pre} (***Figure 8(c)***). This reduction in ultimate mechanical properties with increasing λ_{pre} is the result of chain alignment along the MD in the melt state during the film extrusion process.[55, 56] A previous study by Fu *et al.*[57] showed that the elongation and ultimate tensile strength of pre-oriented HDPE films increased when the angle between pre-orientation direction and stretching direction was altered from 0˚ to 45˚ or 90˚,

which indicated that λ_{max} is also dependent on the solid-state drawing direction. Thus, the draw down or pre-orientation ratio ought not to be chosen too high for the purpose of achieving a high ultimate mechanical performance.

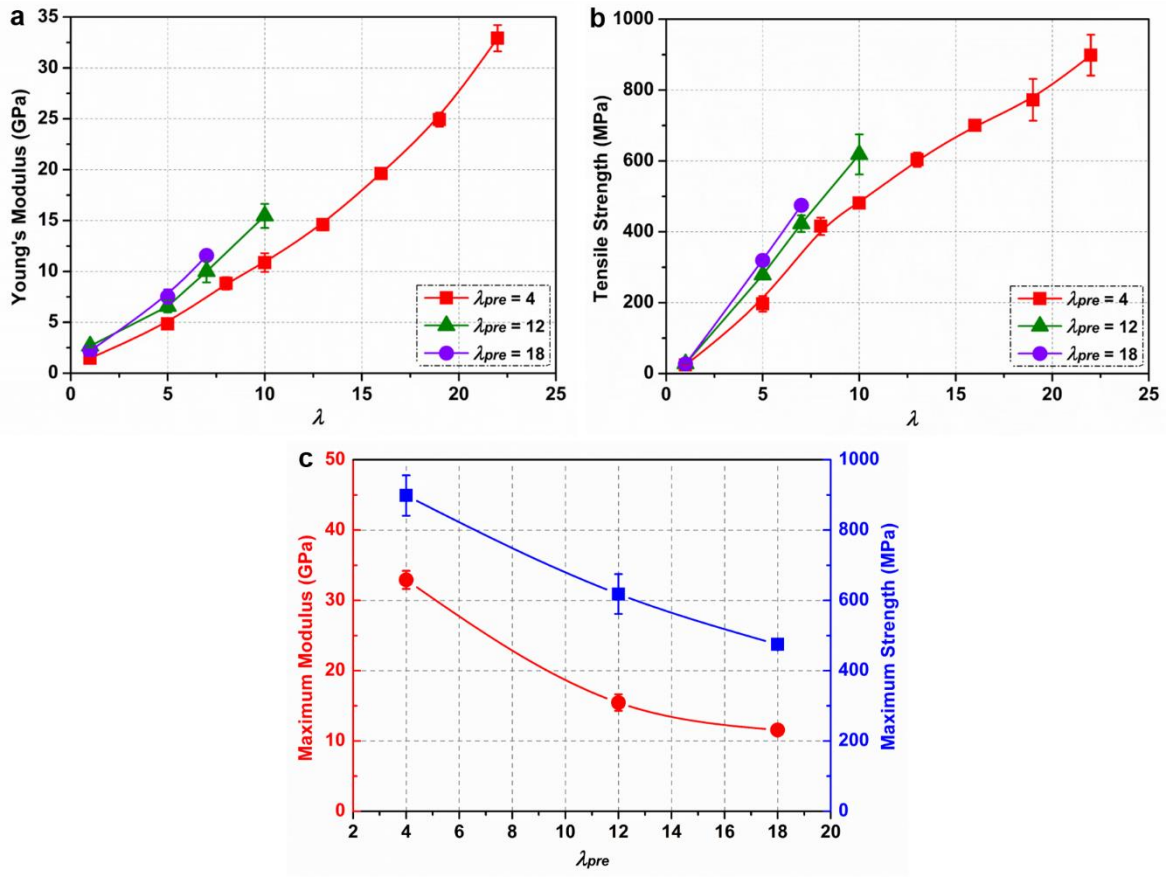

Figure 8. (a) Young's modulus and (b) tensile strength of solid-state drawn HDPE films versus draw ratio with different pre-orientation ratios and (c) maximum modulus and strength of drawn HDPE films as a function of pre-orientation ratio. These results indicate that a high λ_{pre} will lead to better mechanical properties at equal draw ratios but poor ultimate mechanical properties.

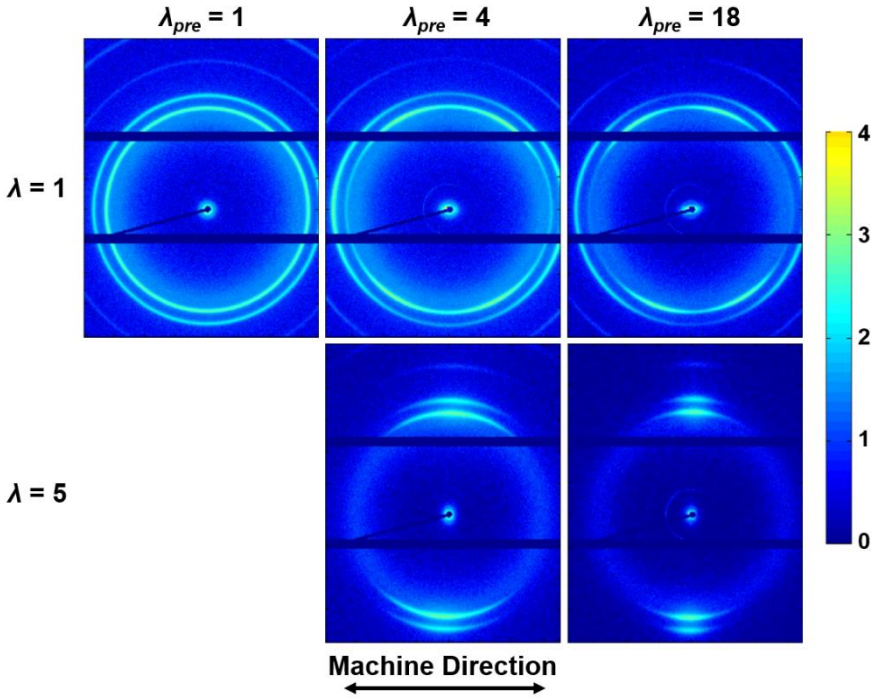

Figure 9. 2D-WAXS patterns of HDPE films with different pre-orientation ratios and draw ratios, showing higher orientation along the MD with increasing λ_{pre} at the same λ.

Table 3. Transmittance at 550 nm of HDPE films with different pre-orientation (λ_{pre}) and draw ratios (λ).

HDPE Films	λ_{pre} **= 4**	λ_{pre} **= 12**	λ_{pre} **= 18**
λ **= 5**	87.6 ± 0.5 %	89.7 ± 0.1 %	89.3 ± 0.4 %
λ **= 7**	88.6 ± 0.3 %	90.0 ± 0.2 %	90.0 ± 0.3 %
λ **= 10**	90.3 ± 0.2 %	90.4 ± 0.1 %	/

It is noteworthy that in the case of HDPE + 2 wt.% BZT, some powders started to appear after 6 months on the surface of the drawn films as shown in ***Figure S3(a)*** and ***S3(b)***. SEM images in combination with EDS analysis corroborated that BZT particles were present on the surface of these HDPE films. As a result, transmittance values of the films dropped by 1−5 % compared to corresponding freshly drawn films (see ***Table S1***). However, the presence of these powders

on the HDPE film surface did not significantly affect the clarity of the final laminates when these films were sandwiched between glass slides and TPU interlayers. Freshly drawn HDPE + 2 wt.% BZT films showed that hardly any BZT particles were present on the surface of these films (see ***Figure S3(c)***) while drawn HDPE films without additives maintained their highly transparent character even after long-term storage (see ***Figure S3(d)***). This phenomenon of BZT powders migrating to the surface of the films after long periods of time implies that BZT is not all that stable and compatible with HDPE. Clearly this is a disadvantage of the BZT based technology, while an additional compounding step before film extrusion is also necessary when using such additives, adding costs compared to a methodology which is merely based on an optimized drawing temperature and draw ratio. In addition, the cost of such additives is usually high. On the whole, it can therefore be concluded that solid-state drawing at an optimal drawing temperature of 105 °C without additives is therefore the preferred method to achieve cost-effective highly transparent HDPE films with excellent mechanical performance.

In terms of applications, these highly transparent, high strength ultra-drawn polyethylene films and tapes could act as reinforcing layers in transparent laminated composites. The realization of a continuous extrusion and solid-state drawing process of these transparent and high strength HDPE films makes their actual applications in fields of transportation and life protection possible, which includes but is not limited to glazing for buildings, automotive vehicles or aircraft, transparent armor, visors, safety glass or displays. Due to their lightweight, high mechanical performance and ease of production at relatively low cost, these films and their laminated composites have great potential as replacements for traditional inorganic glazing and commercial transparent polymeric materials like PC or PMMA. Moreover, such oriented films or tapes could form the basis for a new range of transparent ‘self-reinforced’ or ‘all-polymer’ composites.[58-61]

4. Conclusions

This study successfully demonstrated the potential of a continuous extrusion and solid-state drawing process for the low-cost production of lightweight, transparent, high strength HDPE films and tapes. Two approaches based on solid-state drawing at a temperature of 105 °C with and without the incorporation of BZT as an additive into these oriented HDPE films were used and compared. It was shown that optical and mechanical properties, void content, crystallinity as well as the degree of molecular orientation were similar for both types of HDPE films at equal draw ratios. Both methods resulted in a negligible amount of micro- or nano-voiding after drawing which limited the amount of potential light scattering by such voids, hence leading to films possessing a high transparency of almost 91 % even in the far field within the visible light spectrum. Moreover, these highly drawn films possessed a high maximum Young's modulus of ~ 33 GPa and tensile strength of ~ 900 MPa, which are nearly 15 times higher than those of PC and PMMA and on a weight basis even outperforms structural materials like aluminum or glass-fiber reinforced plastics. The use of a two-step drawing process did not significantly improve the optical and mechanical properties of the films. A high draw down or pre-orientation ratio was, however, beneficial in enhancing modulus and strength at the same draw ratio, but would also lead to a reduction in ultimate mechanical properties of the films. This study showed that, for the studied draw ratios, the use of BZT as an additive to induce transparency in drawn HDPE films is not necessary when drawing is performed at a temperature of 105 °C. In fact, the BZT-free technology will be the preferred technology from a perspective of long-term stability, low cost, easy processing and convenience. These highly transparent solid-state drawn HDPE films and their laminated composites have great potential as replacements for traditional laminated glass as well as commercial transparent polymeric materials, and are of interest for a wide range of applications including windows and glazing, windshields, visors and displays for electronic devices.

Supporting Information

Supporting Information is available from the Wiley Online Library or from the author.

Acknowledgements

The authors gratefully thank Schweitzer-Mauduit International, Inc. (USA) for providing the TPU interlayers. The authors acknowledge Dr. Lihua Shen for interesting discussions on BZT additives. Y. Lin greatly acknowledges financial support by the China Scholarship Council (CSC).

Conflict of Interest

The authors declare no conflict of interest.

Received: ((will be filled in by the editorial staff))
Revised: ((will be filled in by the editorial staff))
Published online: ((will be filled in by the editorial staff))

References

[1] C. W. G. Hall, R. A. Harper, J. P. Snelling, *SAE Transactions* **1998**, *107*, 2416.

[2] P. Cros, E., L. Rota, C. Cottenot, E., R. Schirrer, C. Fond, *J. Phys. IV France* **2000**, *10*, 671.

[3] P. J. Patel, A. J. Hsieh, G. A. Gilde, U.S. Army Research Laboratory, **2006**.

[4] J. S. Stenzler, N. C. Goulbourne, in *Proceedings of the Society for Experimental Mechanics-Sem Annual Conference and Exposition on Experimental and Applied Mechanics*, **2009**.

[5] J. S. Stenzler, N. C. Goulbourne, *Int. J. Impact Eng.* **2011**, *38*, 567.

[6] M. Grujicic, W. C. Bell, B. Pandurangan, *Mater. Des.* **2012**, *34*, 808.

[7] H. M. Abid, Q. H. Shah, M. S. Ibrahim, *International Journal of Applied Engineering Research* **2017**, *12*, 14514.

[8] C. A. Harper, E. M. Petrie, *Plastics materials and processes: a concise encyclopedia*, John Wiley & Sons, **2003**.

[9] P. V. Grant, W. J. Cantwell, H. McKenzie, P. Corkhill, *Int. J. Impact Eng.* **1998**, *21*, 737.

[10] M. Y. Zang, Z. Lei, S. F. Wang, *Computational Mechanics* **2007**, *41*, 73.

[11] X. Zhang, H. Hao, G. Ma, *Int. J. Impact Eng.* **2013**, *55*, 49.

[12] S. M. Walley, *Strain* **2014**, *50*, 470.

[13] S. Chen, M. Zang, D. Wang, S. Yoshimura, T. Yamada, *Compos Part B - Eng* **2017**, *122*, 47.

[14] M. J. N. Jacobs, J. L. J. Van Dingenen, *J. Mater. Sci.* **2001**, *36*, 3137.

[15] C. Y. Tham, V. B. C. Tan, H. P. Lee, *Int. J. Impact Eng.* **2008**, *35*, 304.

[16] A. Tabiei, G. Nilakantan, *Appl. Mech. Rev.* **2008**, *61*, 010801.

[17] Q. Wang, Z. Chen, Z. Chen, *Mater. Des.* **2013**, *46*, 634.

[18] T. G. Zhang, S. S. Satapathy, L. R. Vargas-Gonzalez, S. M. Walsh, *Compos. Struct.* **2015**, *133*, 191.

[19] A. K. Singh, R. J. H. Wanhill, N. Eswara Prasad, in *Aerospace Materials and Material Technologies : Volume 2: Aerospace Material Technologies* (Eds: N.E. Prasad, R.J.H. Wanhill), Springer Singapore, Singapore, 2017, p. 541.

[20] T. Peijs, in *Comprehensive Composite Materials II* (Eds: P.W.R. Beaumont, C.H. Zweben), Elsevier, Oxford, 2018, p. 86.

[21] M. B. Johnson, G. L. Wilkes, A. M. Sukhadia, D. C. Rohlfing, *J. Appl. Polym. Sci.* **2000**, *77*, 2845.

[22] Z. Jiang, Y. Tang, J. Rieger, H.-F. Enderle, D. Lilge, S. V. Roth, R. Gehrke, Z. Wu, Z. Li, X. Li, Y. Men, *Eur. Polym. J.* **2010**, *46*, 1866.

[23] E. Kretzschmar, M. D. Wolkowicz, J.-F. Enderle, D. Lilge, US8029888, **2011**.

[24] D. J. O'Brien, B. Parquette, M. L. Hoey, J. Perry, *Polym. Compos.* **2018**, *39*, 2523.

[25] L. Shen, K. Nickmans, J. Severn, C. W. M. Bastiaansen, *ACS Appl. Mater. Interfaces* **2016**, *8*, 17549.

[26] L. Shen, J. R. Severn, C. W. M. Bastiaansen, WO2017103055, **2017**.

[27] Y. Lin, R. Patel, J. Cao, W. Tu, H. Zhang, E. Bilotti, C. W. M. Bastiaansen, T. Peijs, *Polymer* **2019**, *171*, 180.

[28] Y. Lin, T. Peijs, C. W. M. Bastiaansen, GB1820429.7, **2018**.

[29] G. Capaccio, I. M. Ward, *Polymer* **1974**, *15*, 233.

[30] W. Wu, W. B. Black, *Polym. Eng. Sci.* **1979**, *19*, 1163.

[31] L. Shen, J. Severn, C. W. M. Bastiaansen, *Macromol. Mater. Eng.* **2017**, *302*, 1700003.

[32] M. G. Rosato, D. V. Rosato, *Concise encyclopedia of plastics*, Springer Science & Business Media, **2012**.

[33] M. A. Spalding, A. Chatterjee, *Handbook of Industrial Polyethylene and Technology: Definitive Guide to Manufacturing, Properties, Processing, Applications and Markets Set*, John Wiley & Sons, **2017**.

[34] Y. Li, Y. A. Akpalu, *Macromolecules* **2004**, *37*, 7265.

[35] Y. Lu, Y. Wang, R. Chen, J. Zhao, Z. Jiang, Y. Men, *Macromolecules* **2015**, *48*, 5799.

[36] J. L. Whittaker, R. Balu, R. Knott, L. de Campo, J. P. Mata, C. Rehm, A. J. Hill, N. K. Dutta, N. Roy Choudhury, *Int. J. Biol. Macromol.* **2018**, *114*, 998.

[37] P. H. Hermans, A. Weidinger, *J. Appl. Phys.* **1948**, *19*, 491.

[38] M. Afeworki, P. Brant, A. Lustiger, A. Norman, *Solid State Nucl. Magn. Reson.* **2015**, *72*, 27.

[39] B. Xiong, O. Lame, J. M. Chenal, C. Rochas, R. Seguela, G. Vigier, *Macromolecules* **2015**, *48*, 5267.

[40] M. F. Butler, A. M. Donald, A. J. Ryan, *Polymer* **1997**, *38*, 5521.

[41] T. Peijs, H. A. Rijsdijk, J. M. M. de Kok, P. J. Lemstra, *Compos. Sci. Technol.* **1994**, *52*, 449.

[42] M. B. Rhodes, R. S. Stein, *J. Appl. Phys.* **1961**, *32*, 2344.

[43] Y. Lu, Y. Men, *Macromol. Mater. Eng.* **2018**, *303*, 1800203.

[44] Z. Jiang, R. Chen, Y. Lu, B. Whiteside, P. Coates, Z. Wu, Y. Men, *J. Phys. Chem. B* **2017**, *121*, 6673.

[45] Z. Jiang, Y. Tang, Y. Men, H.-F. Enderle, D. Lilge, S. V. Roth, R. Gehrke, J. Rieger, *Macromolecules* **2007**, *40*, 7263.

[46] Y. Men, J. Rieger, H.-F. Endeler, D. Lilge, *Macromolecules* **2003**, *36*, 4689.

[47] Z. Jiang, Y. Tang, J. Rieger, H.-F. Enderle, D. Lilge, S. V. Roth, R. Gehrke, W. Heckmann, Y. Men, *Macromolecules* **2010**, *43*, 4727.

[48] A. Pawlak, A. Galeski, A. Rozanski, *Prog. Polym. Sci.* **2014**, *39*, 921.

[49] B. Chang, K. Schneider, G. Heinrich, *Macromol. Mater. Eng.* **2017**, *302*, 1700152.

[50] B. Chang, K. Schneider, F. Xiang, R. Vogel, S. Roth, G. Heinrich, *Macromolecules* **2018**, *51*, 6276.

[51] K.-J. Choi, J. E. Spruiell, J. L. White, *J. Polym. Sci., Part B: Polym. Phys.* **1982**, *20*, 27.

[52] W.-G. Hu, K. Schmidt-Rohr, *Acta Polym.* **1999**, *50*, 271.

[53] P. Smith, P. J. Lemstra, *J. Mater. Sci.* **1980**, *15*, 505.

[54] B. Brew, I. M. Ward, *Polymer* **1978**, *19*, 1338.

[55] P. Y. F. Fung, S. H. Carr, *J. Macromol. Sci. B* **1972**, *6*, 621.

[56] X. M. Zhang, S. Elkoun, A. Ajji, M. A. Huneault, *Polymer* **2004**, *45*, 217.

[57] L. Fu, Z. Jiang, H.-F. Enderle, D. Lilge, Z. Wu, S. S. Funari, Y. Men, *J. Polym. Sci., Part B: Polym. Phys.* **2014**, *52*, 716.

[58] T. Peijs, *Mater. Today* **2003**, *4*, 30.

[59] N. Cabrera, B. Alcock, J. Loos, T. Peijs, *Proceedings of the Institution of Mechanical Engineers, Part L: Journal of Materials: Design and Applications* **2004**, *218*, 145.

[60] J. M. Zhang, C. T. Reynolds, T. Peijs, *Compos. Part A - Appl. S.* **2009**, *40*, 1747.

[61] B. Alcock, T. Peijs, in *Polymer Composites – Polyolefin Fractionation – Polymeric Peptidomimetics – Collagens* (Eds: A. Abe, H.-H. Kausch, M. Möller, H. Pasch), Springer Berlin Heidelberg, Berlin, Heidelberg, 2013, p. 1.

Table of Contents

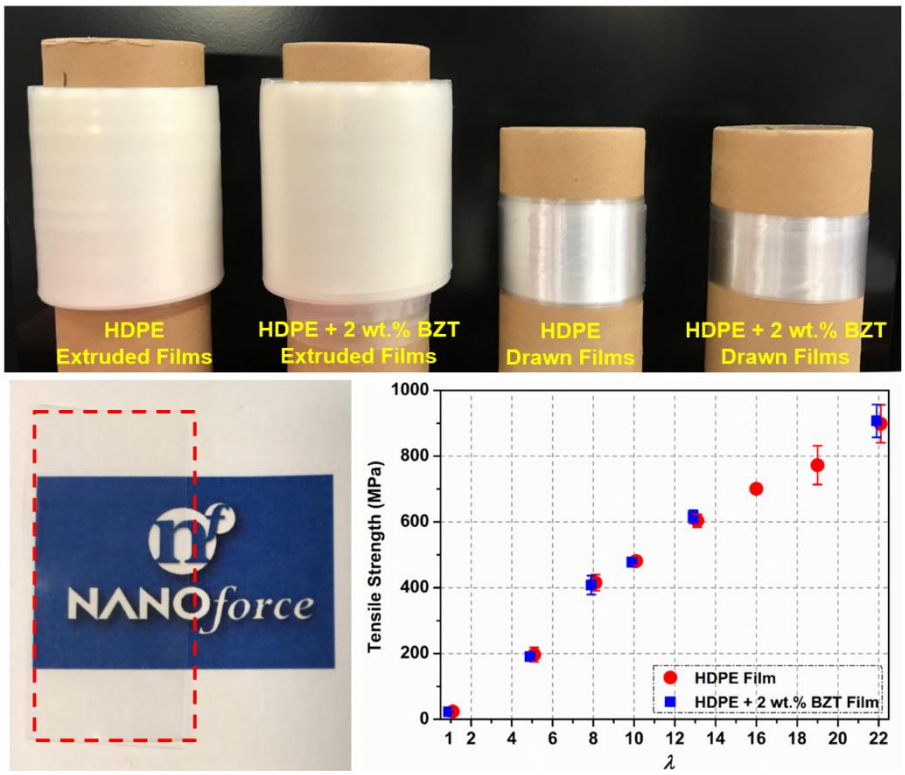

Transparent high strength high-density polyethylene (HDPE) films are manufactured using additive or additive-free technology in a cast film extrusion and solid-state drawing line. These films possess both a high transparency (91 %) and a maximum attainable tensile strength of around 900 MPa. The effect of draw down or pre-orientation in the as-extruded films prior to solid-state drawing is explored.